Bioorganic & Medicinal Chemistry 23 (2015) 6118–6124

Contents lists available at ScienceDirect

Bioorganic & Medicinal Chemistry

journal homepage: www.elsevier.com/locate/bmc

Ridaifen G, tamoxifen analog, is a potent anticancer drug working through a combinatorial association with multiple cellular factors

Kentaro Ikeda [a,†], Shinji Kamisuki [a,†], Shoko Uetake [b], Akihito Mizusawa [b], Nozomi Ota [b], Tatsuki Sasaki [a], Senko Tsukuda [a], Tomoe Kusayanagi [a], Yoichi Takakusagi [a], Kengo Morohashi [c], Takao Yamori [d,‡], Shingo Dan [d], Isamu Shiina [b], Fumio Sugawara [a,*]

[a] Department of Applied Biological Science, Tokyo University of Science, Chiba, Japan
[b] Department of Applied Chemistry, Tokyo University of Science, Tokyo, Japan
[c] Department of Molecular Genetics, The Ohio State University, Columbus, OH, United States
[d] Division of Molecular Pharmacology, Cancer Chemotherapy Center, Japanese Foundation for Cancer Research, Tokyo, Japan

ARTICLE INFO

Article history:
Received 17 July 2015
Revised 31 July 2015
Accepted 1 August 2015
Available online 5 August 2015

Keywords:
Tamoxifen
Anticancer drug
Phage display
Target identification

ABSTRACT

Ridaifen-G (RID-G), a tamoxifen analog that we previously synthesized, has potent growth inhibitory activity against various cancer cell lines. Tamoxifen is an anticancer drug known to act on an estrogen receptor (ER) and other proteins. However, our previous studies interestingly suggested that the mechanism of action of RID-G was different from that of tamoxifen. In order to investigate the molecular mode of action of RID-G, we developed a novel chemical genetic approach that combined a phage display screen with a statistical analysis of drug potency and gene expression profiles in thirty-nine cancer cell lines. Application of this method to RID-G revealed that three proteins, calmodulin (CaM), heterogeneous nuclear ribonucleoproteins A2/B1 (hnRNP A2/B1), and zinc finger protein 638 (ZNF638) were the candidates of direct targets of RID-G. Moreover, cell lines susceptible to RID-G show similar expression profiles of RID-G target genes. These results suggest that RID-G involves CaM, hnRNP A2/B1, and ZNF638 in its growth inhibitory activity.

1. Introduction

Classical cytotoxic anticancer drugs, such as taxol, doxorubicin, and tamoxifen, have been used for cancer chemotherapy. Several reports suggested that these drugs acted on multiple target proteins to exert cytotoxic effects on cancer cells.[1,2] One of them, tamoxifen, has been widely used in chemotherapy against breast cancers. The primary target molecule is known to be ER; however, many studies on the mechanism of action reported that tamoxifen acted not only on ER, but also on other target proteins such as CaM, protein kinase C, and proto-oncogene c-Myc.[3]

Target identification of bioactive compounds can elucidate their molecular mechanism. Although a variety of methodologies for identifying target proteins has been reported, comprehensive identification of multiple target proteins is still difficult.[4] Although chemical proteomics workflow using affinity matrix-based protein purification is often used for target identification, we have employed phage display screen to identify binding proteins of bioactive compounds.[5–8] Compared with chemical proteomics workflow, the phage display screen method has the advantage of identifying multiple targets, since DNA sequencing of the inserts in the phage clones detects numerous binding proteins, whereas liquid chromatography–mass spectrometry analysis of proteins gives relatively little information. Once cDNA libraries derived from several cultured cell lines and tissues are constructed, several types of phage libraries can be used for the screening as libraries of the binding partner. Arango et al. have recently developed a novel approach that combines phage display with next generation sequencing, which allowed the comprehensive identification of human targets of a bioactive flavonoid.[9] Although the phage display screen method is indeed feasible for comprehensive target identification, it still has shortcomings. In particular, the phage display screen method does not provide physiological information on the interaction between a compound and a target protein. In this paper, we propose a unique chemical genetic approach in which phage display screen was combined with a statistical analysis using drug potency and gene expression profiles to understand the physiological relevance of the direct association (Fig. 1).

* Corresponding author. Tel.: +81 4 7124 1501x3400; fax: +81 4 7123 9767.
E-mail address: sugawara@rs.noda.tus.ac.jp (F. Sugawara).
† These authors contributed equally to this work.
‡ Present address: Center for Product Evaluation, Pharmaceuticals and Medical Device Agency, Tokyo, Japan.

http://dx.doi.org/10.1016/j.bmc.2015.08.001
0968-0896/

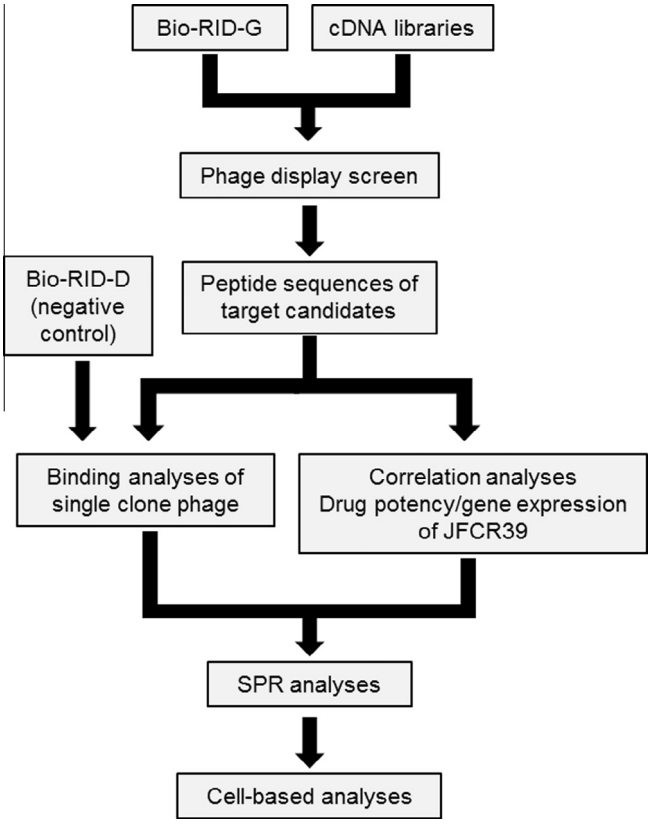

Figure 1. A flowchart showing the identification of proteins for multiple target drugs.

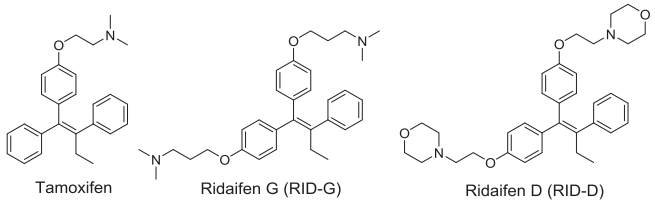

Figure 2. Structures of tamoxifen, RID-G and RID-D.

To demonstrate our strategy, we chose a tamoxifen analog, RID-G (CAS Registry Number 1020853-04-6) as a multi-target drug (Fig. 2). We previously synthesized tamoxifen analogs named ridaifens,[10] and one of them, RID-G, exhibited the highest potency.[11,12] The mean value of GI_{50} (the concentration for 50% of maximal inhibition) over thirty-nine human cancer cell lines (designated as MG-MID) of RID-G was 0.85 μM, while MG-MID of tamoxifen was 7.41 μM.[13] Moreover, GI_{50} profiles across thirty-nine cell lines (designated as JFCR39 by the Japanese Foundation for Cancer Research) suggested that the mode of action of RID-G was ER-independent and different from that of tamoxifen.[13] Since RID-G, like tamoxifen, was expected to affect multiple target proteins to exert cytotoxicity against cancer cells, we applied our strategy on a comprehensive identification of RID-G-binding proteins by using GI_{50}/gene expression profiles of JFCR39 cell lines (Fig. 1). Phage display screen with RID-G-immobilized matrix identified RID-G-binding peptides, and their interactions were validated by binding analyses of each single clone phage. The candidate genes were further analyzed to investigate the relationship of GI_{50} values of RID-G with gene expression profiles in the cell lines. By applying the workflow, we identified CaM, hnRNP A2/B1, and ZNF638 as plausible target proteins of RID-G.

2. Materials and methods

2.1. T7 phage display screen

T7 phage display screening was performed as described in Supporting information. In brief, an aliquot of the T7 phage library was added to control or Bio-RID-G-immobilized well, and the mixture was then incubated for 1 h. After incubation, the wells were washed with TBST (TBS, 0.1% Tween 20). An elution buffer (TBS, 1% SDS) was then added, and the mixture was incubated for 15 min to recover the remaining phage particles. In order to amplify the recovered phage particles, each eluate was mixed with a culture of *Escherichia coli* BLT5615 (Merck Millipore, Billerica, MA, USA). The cells were then cultured at 37 °C until cell lysis was observed. The resulting solution was used for the next round of biopanning. After six rounds of selection, the DNA sequence of each phage clone was then analyzed.

2.2. SPR analysis

SPR analysis was performed on a Biacore® 3000 (GE Healthcare, Buckinghamshire, England). The purified CaM or hnRNP B1 (2–200 a.a.) was immobilized on a CM5 sensor chip. After the immobilization, appropriate concentrations of compounds were injected over the flow cells. Binding analyses were carried out with a flow rate of 20 μL/min at 25 °C. Kinetic parameters were determined by analyzing the data using the BIAevaluation 4.1 software (GE Healthcare).

2.3. Analysis of ERK1/2 phosphorylation level

HeLa cells were cultured in serum-free medium for 48 h and then incubated with RID-G. The cells were harvested, and the cell lysates were mixed with an equal volume of 2× SDS sample buffer. The sample was then heated at 96 °C for 10 min.

2.4. Expression and purification of recombinant hnRNP B1

Expression and purification of recombinant hnRNP B1 was performed as described in Supporting information. In brief, hnRNP B1 (2–200 a.a.) expression vector was used to transform *E. coli* Rosetta 2 (DE3) (Novagen). These bacteria were grown in LB medium and treated with 1 mM isopropyl thio-β-D-galactoside. After incubation for 5 h, the cells were harvested and suspended in a buffer. The cells were disrupted by sonication, and the soluble fraction was loaded onto a HisTrap HP column (GE Healthcare) using an FPLC system (AKTA explorer, GE Healthcare). Finally, bound proteins were eluted using an elution buffer (500 mM NaCl, 8.1 mM Na_2HPO_4, 2.68 mM KCl, 1.47 mM KH_2PO_4, 0.05% Triton X-100, 5% glycerol, 0.5 M imidazole, pH 7.4).

3. Results

3.1. Selection of RID-G-binding proteins using a T7 phage display screen

RID-G and biotinylated RID-G (Bio-RID-G) were synthesized using the Mukaiyama reductive coupling reaction,[14,15] and the Shiina esterification (Fig. S1, Supporting information).[16–18] Since our purpose was to identify RID-G-binding proteins in a comprehensive manner, we used cDNA libraries derived from multiple cell lines such as Jurkat cells (human T-cell leukemia), TE8 cells

Table 1
Peptides displayed on phage clones obtained after the screening

No.	Protein name (region)	Identity (%)
4	WW domain-binding protein 4 (117–250 a.a.)	97
7	Eukaryotic translation initiation factor 4 gamma 1(1079–1171 a.a.)	93.5
8	Cysteine and glycine-rich protein 1 (135–193 a.a.)	98.3
9	Calmodulin (1–75 a.a.)	98.7
10	Zinc finger protein 638 (1313–1479 a.a.)	99.4
11	Ankyrin repeat domain-containing protein 11 (1203–1394 a.a.)	90.8
13	Plasminogen activator inhibitor 1 RNA-binding protein (115–286 a.a.)	96.5
15	Heterogeneous nuclear ribonucleoproteins A2/B1 (14–130 a.a.)	99.1

(human esophageal squamous cell carcinoma), and HUVECs, and human lung tumors. Each T7 phage library was incubated with Bio-RID-G immobilized on wells, and affinity selection was performed. After several rounds of selection, binding phage clones were amplified, and each DNA sequence was analyzed (Table S1, Supporting information). The translated amino acid sequences of sixteen clones were summarized in Table 1. Out of sixteen clones, eight clones (No. 4, 7, 8, 9, 10, 11, 13, and 15) had high homology with human proteins and were further analyzed.

3.2. Binding analyses of single clone phage and gene expression profiles in cancer cell lines

To confirm specific binding of RID-G to each peptide, we performed a binding assay using single clone of T7 phage particles displaying each peptide. Each phage clone was applied to nonimmobilized or Bio-RID-G-immobilized wells, and the recovery rate was calculated (Fig. 3A). Phage clones Nos. 4 and 7 showed lower values for ratios of recovery rates between Bio-RID-G (L)

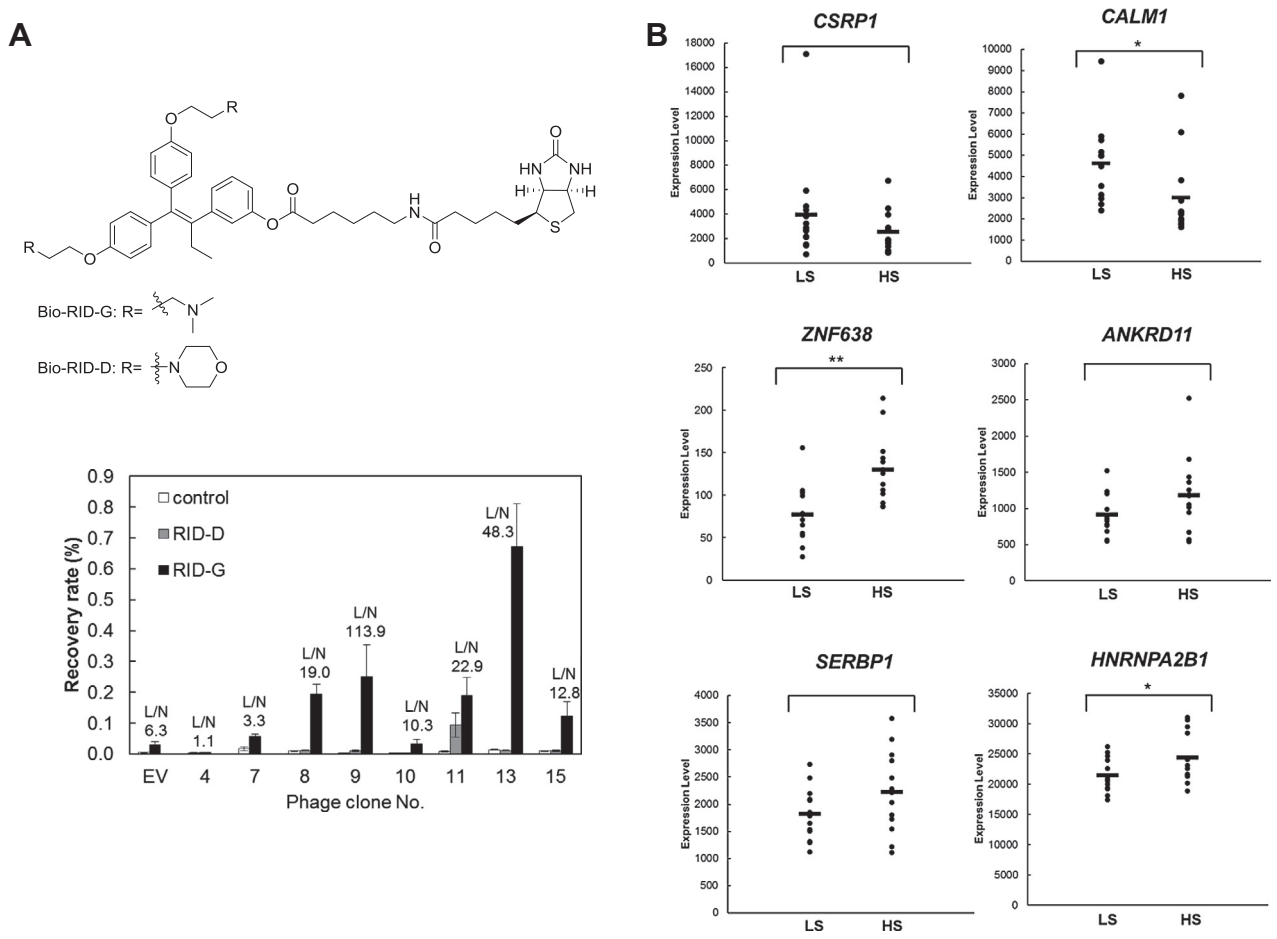

Figure 3. Binding analyses of single clone phage and gene expression profiles in JFCR39 cells. (A) The affinity binding of each single clone to RID-G or RID-D. Each single clone was incubated into the control well, Bio-RID-G- or Bio-RID-D-immobilized well; the phage titer in each eluate was compared to the input phage titer and shown as recovery rate. EV is an empty phage vector. Mean values are shown ± the standard error ($n = 3$). L/N is the ratio between the recovery rates of Bio-RID-G and the control. (B) Correlations between RID-G sensitivity and expression level of gene encoding each RID-G-binding candidate protein. Expression level of five genes, *CSRP1* (cysteine and glycine-rich protein 1), *CALM1* (calmodulin), *ZNF638* (zinc finger protein 638), *ANKRD11* (ankyrin repeat domain-containing protein 11), *SERBP1* (plasminogen activator inhibitor 1 RNA-binding protein) and *HNRNPA2/B1* (heterogeneous nuclear ribonucleoproteins A2/B1) were plotted for two groups (HS group: $GI_{50} < 1.0$ μM and LS group: $GI_{50} > 1.5$ μM). Student's *t* test was used to examine significance of differential expression ($^{*}P < 0.05$; $^{**}P < 0.01$).

and control (N) (L/N) than of phage clones with no insert (EV). These results indicated that peptides displayed by phage clones Nos. 4 and 7 had low affinity with RID-G; thus, we eliminated these clones from the RID-G-binding candidate proteins. We also used ridaifen D (RID-D) (CAS Registry Number 939819-26-8) (Fig. 3A) as a negative control, whose cytotoxicity was lower than that of RID-G; MG-MID of RID-D was 14.8 μM, whereas that of RID-G was 0.85 μM.[13] Recovery rates of clones Nos. 8, 9, 10, 13 and 15 with Bio-RID-G were significantly higher than those with Bio-RID-D, whereas the difference in the affinity of clone No. 11 for Bio-RID-G and for Bio-RID-D was not statistically significant ($P > 0.05$). Thus, the peptide displayed by phage clone No. 11 (ankyrin repeat domain-containing protein 11) was unlikely to be involved in RID-G cytotoxicity. Therefore, we focused on five clones, No. 8 (cysteine and glycine-rich protein 1), No. 9 (CaM), No. 10 (ZNF638), No. 13 (plasminogen activator inhibitor 1 RNA-binding protein), and No. 15 (hnRNP A2/B1) for further analysis.

Next, the correlation between RID-G cytotoxicity and gene expression was determined using the expression level of each gene, which may encode the candidate of RID-G-binding proteins. The cytotoxicity of RID-G in JFCR39 cell lines had been previously evaluated,[13] and the expression level of each gene in the JFCR39 cell lines was determined by DNA microarray (unpublished data). Thirty-nine cell lines in the JFCR39 collection were divided into two groups: high sensitivity group (designated as 'HS') and low sensitivity group (designated as 'LS') for the treatment of RID-G. The cells with $GI_{50} < 1.0$ μM were classified as HS, whereas the cells with $GI_{50} > 1.5$ μM as LS. The expression levels of candidates *CSRP1*, *CALM1, ZNF638, SERBP1,* and *HNRNPA2/B1* and of the nonspecific binding protein *ANKRD11* were plotted in each group (Fig. 3B). As a result, three genes (*CALM1, HNRNPA2B1*, and *ZNF638*) were differentially expressed between the HS and LS groups ($P < 0.05$), whereas *CSRP1*, *SERBP1*, and *ANKRD11* were not ($P > 0.05$). *CALM1* gene expression was high in the LS group, whereas the other two genes were high in the HS group. The expression of *ANKRD11* was not significantly different between the two groups, which was consistent with the binding analysis of single clone phage (No. 11) for Bio-RID-G and Bio-RID-D (Fig. 3A). Five irrelevant genes (e.g., *TUBB*) were also analyzed by the same method and found to be not significantly different between the two groups with different sensitivities to the RID-G treatment (data not shown). These data suggested that the three genes encoding the proteins CaM, hnRNPA2/B1, and ZNF638 were involved in RID-G-mediated inhibition of cancer cell proliferation. Considering the single-clone binding assay and the correlation analysis, we hypothesized that RID-G could bind to the three proteins and modulate their functions, thus exerting cytotoxicity. Therefore, we further analyzed these proteins.

3.3. Effect of RID-G on CaM

Tamoxifen has been also known to be a CaM antagonist.[3] Considering the structural similarity between RID-G and tamoxifen, CaM is the most reliable candidate among the target proteins. CaM is a major calcium-binding protein that is responsible for the regulation of a wide range of cellular signaling. Upon the binding of Ca^{2+} to the EF-hand motif of CaM, its conformation change occurs, allowing the interaction with several Ca^{2+}–CaM target proteins.[19] Since the phage clone No. 9 contains a calcium binding region of CaM, we investigated whether the binding of RID-G with phage clone No. 9 was Ca^{2+}-dependent by performing single-clone binding assay in the presence of EGTA, a Ca^{2+} chelator as described previously (Fig. 4A).[20] The addition of EGTA remarkably decreased the binding of Bio-RID-G to the CaM peptide displayed on phage particles, and the binding was recovered by adding an excess of Ca^{2+}. These data indicated that Ca^{2+} was essential for the binding between RID-G and CaM.

We further analyzed the affinity of RID-G to CaM by surface plasmon resonance (SPR) method (Fig. 4B). Various concentrations of RID-G were injected on the surface of the CM5 sensor chip where CaM proteins had been immobilized. In the presence of Ca^{2+}, RID-G bound to CaM in a dose-dependent manner, and the K_D value obtained by global fitting was 4 μM. The binding was impaired by the addition of EGTA, which was consistent with the single-clone binding assay (Fig. 4A). We also compared the affinity of RID-G with that of tamoxifen (Fig. 4B). Interestingly, tamoxifen showed low affinity binding to CaM in our SPR experiment, suggesting that the affinity of RID-G was higher than that of tamoxifen.

Considering the high affinity of RID-G to Ca^{2+}–CaM and the known CaM antagonist property of tamoxifen, we hypothesized that RID-G could function as a CaM antagonist in cells. Several CaM antagonists are known to activate ERK, a critical mediator of Ca^{2+}–CaM signaling, and to suppress cancer cell proliferation.[20] To clarify whether the binding of RID-G with Ca^{2+}–CaM could have an antiproliferative activity against cancer cells, we examined phosphorylation levels of ERK1/2 in HeLa cells. HeLa cells showed moderate sensitivity to RID-G with an IC_{50} value of 2.4 μM (Fig. S2, Supporting information). HeLa cells were treated with RID-G, and the phosphorylation level of ERK1/2 was assessed. As a result, RID-G induced phosphorylation of ERK1/2, and the phosphorylation was sustained up to 2 h, which was consistent with the property of known CaM antagonists (Fig. 4C).[20] The increase in ERK1/2 phosphorylation was also observed in the presence of FBS (Fig. 4D). These data suggested that RID-G bound to Ca^{2+}–CaM to inhibit its signaling in cancer cells.

3.4. Binding analyses of RID-G to hnRNPA2/B1

HnRNP A2/B1 is a member of the hnRNP family known as a splicing factor and has been reported to be highly expressed in many cancers.[21–24] Knockdown of this protein induces cell death by apoptosis in various cancer cells, but not in normal cells.[25] Therefore, RID-G–hnRNP A2/B1 interaction can be involved in RID-G-mediated cytotoxicity against cancer cells. To confirm the interaction, SPR analysis using a recombinant hnRNP A2/B1 peptide was performed. His-tagged N-terminal region of hnRNP A2/B1 (hnRNP A2/B1 [2–200 a.a.]) corresponding to the region displayed on the RID-G-binding phage particles was purified and used for SPR analysis. As a result, the response was increased in a dose-dependent manner after adding RID-G, and the K_D value was 3 μM (Fig. 5). Since this K_D value was comparable to that of CaM (4 μM) and to the GI_{50} value of RID-G (0.85 μM), the binding of RID-G to hnRNP A2/B1 might partially inhibit cancer cell growth.

4. Discussion

In this paper, we have identified three proteins, CaM, hnRNPA2/B1, and ZNF638 as candidate target proteins of RID-G, a tamoxifen analog, by T7 phage display screen. The validation of target proteins is generally a time-consuming process. In this study, candidates obtained from phage display screen were subjected to two analyses: (1) single-clone binding assay using RID-D as a negative control compound without biological activity, and (2) a statistical analysis of the gene expression profiles combined with RID-G cytotoxicity. The chemical genetic approach could be useful for the identification of multiple target proteins of small molecules, especially multi-target drugs such as tamoxifen.

We demonstrated that RID-G had higher affinity for CaM than tamoxifen and acted as a CaM antagonist in cells, like tamoxifen

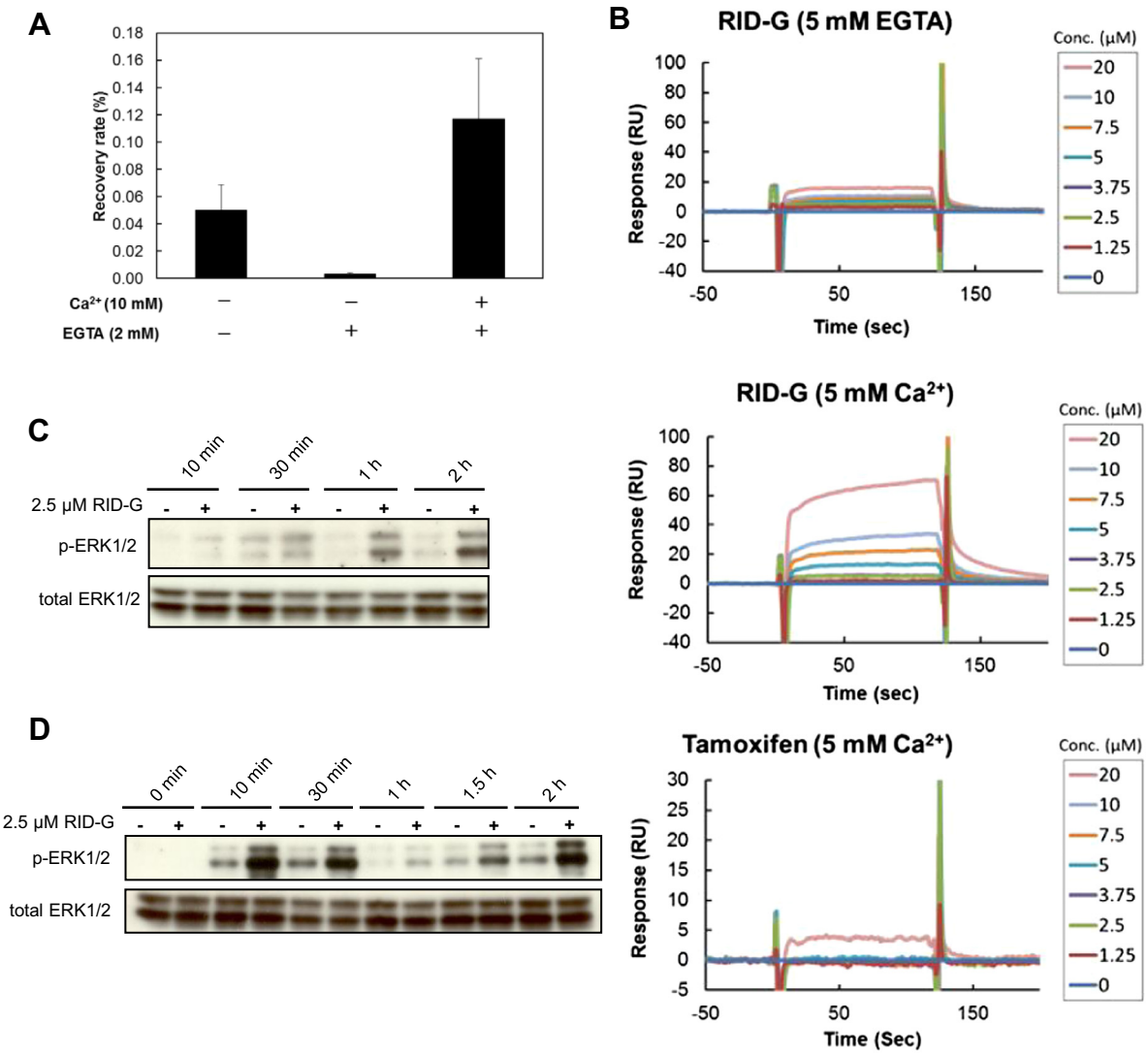

Figure 4. Effect of RID-G on calmodulin (CaM). (A) Effect of Ca^{2+} and EGTA on the binding of RID-G to single phage clones displaying CaM (1–75 a.a.). The phage particles were incubated with Bio-RID-G in the presence or absence of 2 mM EGTA with or without excess amount of Ca^{2+} (10 mM), and the recovery rates were calculated. Mean values are shown ± the standard error (n = 3). (B) SPR analysis of RID-G or tamoxifen binding to CaM. CaM was immobilized on a flowpath of CM5 sensorchip, and a solution of RID-G or tamoxifen at indicated concentrations was injected to protein-immobilized flowpath in the presence of 5 mM EGTA or 5 mM Ca^{2+}. The binding responses (in RU) were recorded as a function of time (in sec), and the results were analyzed by using BIA evaluation 4.1. (C) and (D) Effect of RID-G on ERK 1/2 phosphorylation. HeLa cells were starved in medium without FBS for 48 h and then treated with 2.5 μM RID-G in the absence (C) or presence (D) of 10% FBS for the indicated time points. An anti-phospho ERK 1/2 antibody was used to detect ERK 1/2 phosphorylation (p-ERK 1/2). The protein levels of ERK 1/2 were used as internal controls (total ERK 1/2).

(Fig. 4). However, a previous study showed that ER-binding activity of RID-G was lower than that of tamoxifen.[13] These differences in the affinities could explain a distinct mechanism of action between RID-G and tamoxifen.[13] Recently, it was reported that tamoxifen disrupted CaM–Fas interaction,[26] and several CaM antagonists and tamoxifen induced apoptosis through a Fas-related mechanism in cholangiocarcinoma and other cancer cell lines.[27–29] Our result suggested that higher expression of CaM decreased sensitivity of cancer cells to RID-G (Fig. 3B). Therefore, CaM is the most reliable target among the selected proteins because related to RID-G-mediated cytotoxicity.

We have also identified other two candidate proteins, hnRNP A2/B1 and ZNF638. HnRNP A2/B1 is known to be highly expressed in many cancers and regulate splicing of oncogenes. Our SPR analysis demonstrated that RID-G had a similar affinity for hnRNP A2/B1 as for CaM (Fig. 5). Additionally, gene expression profiles in cell lines affected by RID-G suggested that the cancer cell lines expressing hnRNP A2/B1 at relatively higher levels were likely to be sensi-

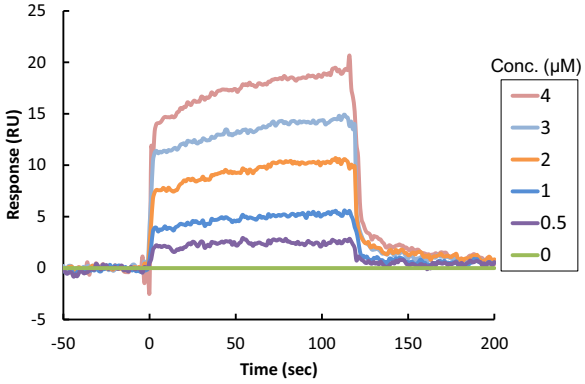

Figure 5. SPR analysis of the binding of RID-G to hnRNPA2/B1. HnRNPA2/B1 was immobilized on a flowpath of CM5 sensorchip, and a solution of RID-G at indicated concentrations was injected to the protein-immobilized flowpath. The binding responses (in RU) were recorded as a function of time (in sec), and the results were analyzed by using BIA evaluation 4.1.

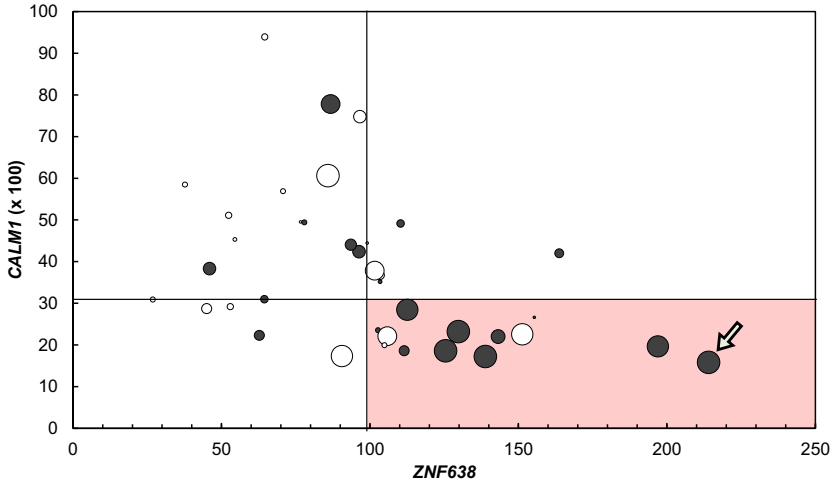

Figure 6. Correlation map of the expression levels of CaM, hnRNP A2/B1, and ZNF638, and the GI_{50} of RID-G. Horizontal and longitudinal axes indicate *ZNF638* and *CALM1* expression levels, respectively. The colors of each circle, white and black, indicate *HNRNPA2B1* expression level. White or black circle represents a lower or higher expression level, comparing to the intermediate value of *HNRNPA2B1* expression levels in JFCR39 cell lines. The red area indicates a lower *CALM1*expression level and a higher *ZNF638* expression level using as reference the intermediate value of each protein expression level in JFCR39 cell line. The circle size indicates the GI_{50} values of RID-G (the smaller one shows a weaker effect and the bigger one shows a stronger effect). The arrow indicates the DMS114 cell line, showing the lowest GI_{50} among the JFCR39 cell lines.

tive to RID-G treatment (Fig. 3B). It can be speculated that RID-G might be able to impair splicing activity of hnRNP A2/B1 through direct binding and block aberrant proliferation of cancer cells dependent on hnRNP A2/B1 overexpression. Golan-Gerstl et al. revealed that hnRNP A2/B1 regulated alternative splicing of tumor suppressors and oncogenes in glioblastoma.[30] Therefore, hnRNPA2/B1 is a potential new target for glioblastoma and other cancers therapy. Although the effects of RID-G on hnRNPA2/B1 cellular function still remain to be investigated, RID-G could be a potential new anticancer drug targeting hnRNP A2/B1.

There are few reports on cellular functions of ZNF638; Mueller and co-workers recently reported that ZNF638 played a role as a transcriptional coregulator of adipocyte differentiation via induction of peroxisome proliferator-activated receptor γ, and ZNF638 also interacts with splicing regulators to influence alternative splicing.[31,32] To examine the interaction between RID-G and ZNF638, we attempted to express a recombinant ZNF638 peptide in *E. coli*. However, because ZNF638 peptide might be toxic for *E. coli*, we failed to obtain the recombinant peptide. Although further studies to determine the binding are needed in the future, the statistical analysis of gene expression profiles and cytotoxicity suggested that cancer cell lines expressing high levels of ZNF638 were clearly sensitive to RID-G treatment (Fig. 3B).

Considering all our data collectively, we hypothesized that RID-G could bind to the three proteins and modulate their activity to elicit its cytotoxicity against cancer cells. Expression profiles of the three proteins in the JFCR39 cell lines were used to make a correlation map, as shown in Figure 6. The red area indicates the cell lines with a low *CALM1* expression level and a high *ZNF638* expression level, and black circle represent cell lines with a high *HNRNPA2B1* expression level. Our correlation analysis of gene expression with RID-G cytotoxicity suggested that cells expressing *CALM1* at a low level and *HNRNPA2B1* and *ZNF638* at a high level were expected to be relatively sensitive to RID-G treatment (Fig. 3B). Indeed, cell lines shown as black circles in the red area had relatively low GI_{50} values and are designated as larger circles. The DMS114 cell line (lung cancer, indicated by an arrow), satisfied all the three conditions. Interestingly, this cell line was the most sensitive to RID-G treatment among the JFCR39 cell lines with the lowest GI_{50} value (0.19 μM). This correlation map may enable us to predict RID-G effectiveness in other cancer cells by measuring the expression levels of the three genes.

Our approach could be applied for multi-target anticancer drugs, aiming at tailor-made medicine in the future. Once the proteins associating to multi-target drugs are identified by our phage display screen strategy, and the profiles of growth inhibition activities of the drugs against a panel of cell lines are determined, it is possible to make a correlation map using gene expression levels of the target proteins obtained. Eventually, this map would be useful to predict drug effectiveness for clinical usage.

5. Conclusions

In summary, we have identified three proteins, CaM, hnRNPA2/B1, and ZNF638 as candidate target proteins of RID-G, a tamoxifen analog, by a chemical genetic approach. In this approach, we combine phage display screen with a statistical analysis using gene expression profiles of JFCR39 cell lines. Our results suggest that RID-G binds to the three proteins and modulates their functions to exert cytotoxicity against cancer cells.

Acknowledgements

This work was supported by a Health and Labour Sciences Research Grants from the Ministry of Health, Labour and Welfare, Japan to I.S. (11103425).

Supplementary data

Supplementary data associated (amino acid sequences and frequency displayed on phage clones after the screening, synthetic scheme of RID-G and Bio-RID-G, cytotoxicity of RID-G against HeLa cells, supplementary materials and methods, ^{1}H and ^{13}C NMR spectra for all novel compounds) with this article can be found, in the online version, at http://dx.doi.org/10.1016/j.bmc.2015.08.001.

References and notes

1. Aoki, S.; Morohashi, K.; Sunoki, T.; Kuramochi, K.; Kobayashi, S.; Sugawara, F. *Bioconjugate Chem.* **2007**, *18*, 1981.

2. Kusayanagi, T.; Tsukuda, S.; Shimura, S.; Manita, D.; Iwakiri, K.; Kamisuki, S.; Takakusagi, Y.; Takeuchi, T.; Kuramochi, K.; Nakazaki, A.; Sakaguchi, K.; Kobayashi, S.; Sugawara, F. *Bioorg. Med. Chem.* **2012**, *20*, 6248.
3. Mandlekar, S.; Kong, A. N. *Apoptosis* **2001**, *6*, 469.
4. Tashiro, E.; Imoto, M. *Bioorg. Med. Chem.* **2012**, *20*, 1910.
5. Tsukuda, S.; Kusayanagi, T.; Umeda, E.; Watanabe, C.; Tosaki, Y.; Kamisuki, S.; Takeuchi, T.; Takakusagi, Y.; Shiina, I.; Sugawara, F. *Bioorg. Med. Chem.* **2013**, *21*, 311.
6. Takakusagi, Y.; Takakusagi, K.; Sugawara, F.; Sakaguchi, K. *Expert Opin. Drug Discovery* **2010**, *5*, 361.
7. Morohashi, K.; Sahara, H.; Watashi, K.; Iwabata, K.; Sunoki, T.; Kuramochi, K.; Takakusagi, K.; Miyashita, H.; Sato, N.; Tanabe, A.; Shimotohno, K.; Kobayashi, S.; Sakaguchi, K.; Sugawara, F. *PLoS One* **2011**, *6*, e18285.
8. Shimura, S.; Ishima, M.; Nakajima, S.; Fujii, T.; Himeno, N.; Ikeda, K.; Izaguirre-Carbonell, J.; Murata, H.; Takeuchi, T.; Kamisuki, S.; Suzuki, T.; Kuramochi, K.; Watashi, K.; Kobayashi, S.; Sugawara, F. *J. Am. Chem. Soc.* **2013**, *135*, 18949.
9. Arango, D.; Morohashi, K.; Yilmaz, A.; Kuramochi, K.; Parihar, A.; Brahimaj, B.; Grotewold, E.; Doseff, A. I. *Proc. Natl. Acad. Sci. U.S.A.* **2013**, *110*, E2153.
10. Shiina, I.; Sano, Y.; Nakata, K.; Kikuchi, T.; Sasaki, A.; Ikekita, M.; Hasome, Y. *Bioorg. Med. Chem. Lett.* **2007**, *17*, 2421.
11. Anlifeire, A.; Hatori, M.; Morita, A.; Shiina, I.; Nakata, K.; Tosaki, Y.; Wang, Y.-W.; Ikekita, M.; Li, G. *Chin. J. Cell Biol.* **2011**, *33*, 635.
12. Shiina, I. *Jpn. Kokai Tokkyo Koho* (24 April 2008), JP2008094836.
13. Guo, W. Z.; Wang, Y.; Umeda, E.; Shiina, I.; Dan, S.; Yamori, T. *Biol. Pharm. Bull.* **2013**, *36*, 1008.
14. Yu, D.; Forman, B. *J. Org. Chem.* **2003**, *68*, 9489.
15. Mukaiyama, T. *Angew. Chem., Int. Ed. Engl.* **1977**, *16*, 817.
16. Shiina, I.; Ibuka, R.; Kubota, M. *Chem. Lett.* **2002**, 286.
17. Shiina, I.; Kubota, M.; Oshiumi, H.; Hashizume, M. *J. Org. Chem.* **2004**, *69*, 1822.
18. Shiina, I.; Fukui, H.; Sasaki, A. *Nat. Protoc.* **2007**, *2*, 2312.
19. Zhang, M.; Tanaka, T.; Ikura, M. *Nat. Struct. Biol.* **1995**, *2*, 758.
20. Shim, J. S.; Lee, J.; Park, H. J.; Park, S. J.; Kwon, H. J. *Chem. Biol.* **2004**, *11*, 1455.
21. Zhou, J.; Allred, D. C.; Avis, I.; Martínez, A.; Vos, M. D.; Smith, L.; Treston, A. M.; Mulshine, J. L. *Breast Cancer Res. Treat.* **2001**, *66*, 217.
22. Yan-Sanders, Y.; Hammons, G. J.; Lyn-Cook, B. D. *Cancer Lett.* **2002**, *183*, 215.
23. Lee, C. L.; Hsiao, H. H.; Lin, C. W.; Wu, S. P.; Huang, S. Y.; Wu, C. Y.; Wang, A. H.; Khoo, K. H. *Proteomics* **2003**, *3*, 2472.
24. Lee, C. H.; Lum, J. H.; Cheung, B. P.; Wong, M. S.; Butt, Y. K.; Tam, M. F.; Chan, W. Y.; Chow, C.; Hui, P. K.; Kwok, F. S.; Lo, S. C.; Fan, D. M. *Proteomics* **2005**, *5*, 1160.
25. Patry, C.; Bouchard, L.; Labrecque, P.; Gendron, D.; Lemieux, B.; Toutant, J.; Lapointe, E.; Wellinger, R.; Chabot, B. *Cancer Res.* **2003**, *63*, 7679.
26. Fernandez, T. F.; Samal, A. B.; Bedwell, G. J.; Chen, Y.; Saad, J. S. *J. Biol. Chem.* **2013**, *288*, 21898.
27. Ahn, E. Y.; Pan, G.; Oh, J. H.; Tytler, E. M.; McDonald, J. M. *Am. J. Pathol.* **2003**, *163*, 2053.
28. Pawar, P.; Ma, L.; Byon, C. H.; Liu, H.; Ahn, E. Y.; Jhala, N.; Arnoletti, J. P.; McDonald, J. M.; Chen, Y. *Clin. Cancer Res.* **2009**, *15*, 1288.
29. Vickers, S. M.; Jhala, N. C.; Ahn, E. Y.; McDonald, J. M.; Pan, G.; Bland, K. I. *Ann. Surg.* **2002**, *235*, 872.
30. Golan-Gerstl, R.; Cohen, M.; Shilo, A.; Suh, S. S.; Bakàcs, A.; Coppola, L.; Karni, R. *Cancer Res.* **2011**, *71*, 4464.
31. Du, C.; Ma, X.; Meruvu, S.; Hugendubler, L.; Mueller, E. *J. Lipid Res.* **2014**, *55*, 1886.
32. Meruvu, S.; Hugendubler, L.; Mueller, E. *J. Biol. Chem.* **2011**, *286*, 26516.